AD-A109 831 NAVAL RESEARCH LAB WASHINGTON DC F/G 4/1
A TIME-DEPENDENT THREE-DIMENSIONAL SIMULATION OF THE EARTH'S MA--ETC(U)
DEC 81 S H BRECHT, J G LYON, J A FEDDER
UNCLASSIFIED NRL-MR-4690 NL

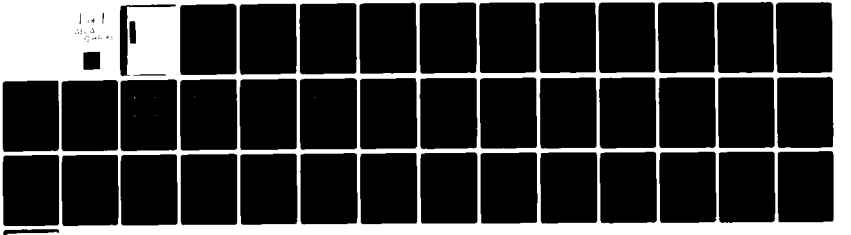

END
DATE FILMED
2-82
DTIC

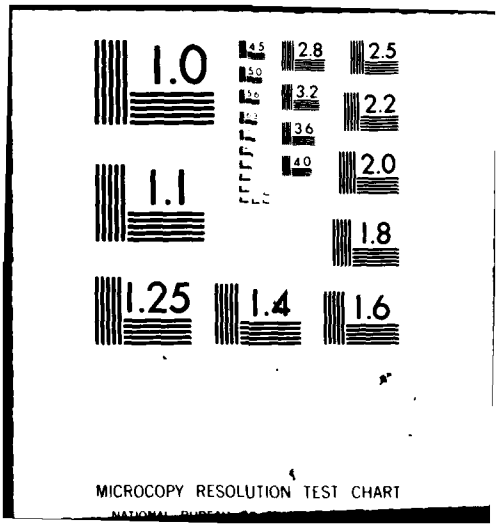
1.0
1.1
1.25
1.4
1.6
1.8
2.0
2.2
2.5
2.8
3.2
3.6
4.0
4.5
5.0
MICROCOPY RESOLUTION TEST CHART

SECURITY CLASSIFICATION OF THIS PAGE (When Data Entered)

REPORT DOCUMENTATION PAGE		READ INSTRUCTIONS BEFORE COMPLETING FORM
1. REPORT NUMBER NRL Memorandum Report 4690	2. GOVT ACCESSION NO. AD-A109 831	3. RECIPIENT'S CATALOG NUMBER
4. TITLE (and Subtitle) A TIME-DEPENDENT THREE-DIMENSIONAL SIMULATION OF THE EARTH'S MAGNETOSPHERE: RECONNECTION EVENTS		5. TYPE OF REPORT & PERIOD COVERED Interim report on a continuing NRL problem. 6. PERFORMING ORG. REPORT NUMBER
7. AUTHOR(s) Stephen H. Brecht*, John G. Lyon*, Joel A Fedder and K. Hain		8. CONTRACT OR GRANT NUMBER(s)
9. PERFORMING ORGANIZATION NAME AND ADDRESS Naval Research Laboratory Washington, DC 20375		10. PROGRAM ELEMENT, PROJECT, TASK AREA & WORK UNIT NUMBERS 61153N; RR0330244; W14365; 47-0884-02 & 1447-01
11. CONTROLLING OFFICE NAME AND ADDRESS		12. REPORT DATE December 22, 1981 13. NUMBER OF PAGES 40
14. MONITORING AGENCY NAME & ADDRESS(if different from Controlling Office) Office of Naval Research McLean, VA 22217 NASA Washington, DC 20546		15. SECURITY CLASS. (of this report) UNCLASSIFIED 15a. DECLASSIFICATION/DOWNGRADING SCHEDULE

16. DISTRIBUTION STATEMENT (of this Report)

Approved for public release; distribution unlimited.

17. DISTRIBUTION STATEMENT (of the abstract entered in Block 20, if different from Report)

18. SUPPLEMENTARY NOTES

*Present address: Science Applications, Inc., McLean, VA 22102.

This work was supported by the Office of Naval Research and NASA.

19. KEY WORDS (Continue on reverse side if necessary and identify by block number)

Magnetic substorm
3-D magnetosphere
Reconnection dynamics
Magnetotail dynamics

20. ABSTRACT (Continue on reverse side if necessary and identify by block number)

This paper presents the results of a 3-D simulation of the earth's magnetosphere. The simulation region covered $-100\ R_e < X < 30\ R_e$, $|Y| \leq 40\ R_e$ and $|Z| \leq 40\ R_e$. The solar wind parameters were $B_z = -2\gamma$, density of 5 cm^{-3} and velocity of 400 km sec^{-1}. The results show the existence of multiple x-points in the tail. Strong plasma flow is seen to exist in both earthward and tailward directions during formation of neutral lines. The exact magnetic field and plasma behavior is found to be very position dependent.

DD FORM 1 JAN 73 1473 EDITION OF 1 NOV 65 IS OBSOLETE
S/N 0102-014-6601

SECURITY CLASSIFICATION OF THIS PAGE (When Data Entered)

A TIME-DEPENDENT THREE-DIMENSIONAL SIMULATION OF THE EARTH'S MAGNETOSPHERE: RECONNECTION EVENTS

Introduction

Time dependent global simulations of the earth's magnetosphere have been performed for several years. The purpose of such a simulation has been and still is to obtain information concerning the general topological structure of the earth's magnetosphere and to address possible cause and effect relationships leading to dynamic phenomena such as magnetic substorms. These large scale calculations can also be used as boundary condition calculations for investigation into the relevant microphysics that produce small scale, but important effects. Finally it is hoped that, as an additional benefit, large scale time dependent simulations might provide further insight into magnetospheric dynamics, so that experimental data might be correlated with the calculation, and a better understanding of the earth's magnetosphere could be reached.

The global simulations to be discussed below all have one thing in common. They are time dependent solutions of the MHD equations. Other than boundary conditions, none of these calculations assumes a particular structure for the magnetosphere nor do they have any adjustable parameters to affect the structure. The number of ad hoc assumptions is held to those required for the validity of the MHD equations. Customarily in a model, macroscopic structure may be manipulated, e.g., the magnetopause boundary might be positioned at will. In these simulations, only the microscopic structure - the underlying physics - is determined. The macroscopic structure then either fits what it is being simulated, or it does not. While questions of accuracy of solution are always important, what the simulations test is whether the physics embodied in the equations solved is adequate to explain the simulated system.

Manuscript submitted October 9, 1981.

Initially only two-dimensional simulations of the magnetosphere were performed; LeBoeuf et al. (1978), Lyon et al. (1980, 1981a). LeBoeuf et al. (1978) used a fluid particle approach in the MHD modeling and were able to reproduce a Dungey (1961) type magnetosphere using the very resistive Lax algorithm, Lax (1954). Lyon et al. (1980), solving the standard MHD equations using a combination of flux corrected transport (Boris and Book, 1973; Zalesak, (1979), and partial donor cell method, (PDM) Hain (1978), addressed the very dynamic problem of, shock focusing. In this work they studied the effect of solar shocks on the earth's magnetosphere. It was found that solar shocks interacted with the magnetosphere in such a way as to focus the shock in the tail region at -15 to -20 R_e. This focusing produced increased temperature and pressures in this region. It was speculated in this paper, as well as in Brecht et al., (1980), that such effects might well trigger magnetic substorms. In addition, Lyon et al. (1981a) studied the problem of substorm-like events triggered by southward directed IMF. For this problem a code was developed that used a leap-frog time-integration scheme and 20^{th} order finite-difference approximation to the spatial derivatives along with a flux-convected transport algorithm (Boris and Book, 1973, Zalesak, 1979) which provides the minimum possible numerical dissipation consistant with a solution showing no extraneous extrema. The results of these simulations produced behavior in the tail which tended to support the neutral-line model for magnetic substorms (Dungey, 1961; Hones, 1973, and McPherron et al, 1973). Research is continuing into the 2-D modeling, particularly with regard to resistive reconnection and how it might be affected by variations in the solar wind.

However, the earth's magnetosphere is a three-dimensional entity. The need to consider it as such has been discussed by many authors, most recently by Akasofu et. al. (1978), Lui et al., (1978), Fairfield (1979), and Coroniti et al. (1980). These authors, to mention a few, have presented considerable evidence that two-dimensional models of the earth's magnetosphere are incomplete. This is in part due to the variability and three-dimensional nature of the solar wind, particularly the Interplanetary Magnetic Field (IMF) carried by the wind. Within the last year, three-dimensional codes have been constructed and the results of their initial work reported; (Leboeuf et al., 1981; Brecht et al., 1981, and Wu et al., 1981). These three simulations considered three somewhat different problems. The first calculation was by LeBoeuf et al. (1981). In this simulation a southward IMF interacted with a current loop. The calculation used periodic bounding conditions and a particle fluid approach with a Lax scheme to solve the MHD equations. The calculation was reported to reproduce a Dungey (1961) like magnetosphere. Unfortunately, the scheme was so diffusive that close inspection of the published magnetic field vector plots reveal no obvious northward field such as one expects to see near the earth's dipole field. The code also had limited spatial extent in the y, z direction causing the possibility of boundary effects to be of concern. The strong numerical diffusion in addition to causing eradication of some, if not all, of the dipole field also prevents the studying of any dynamics of reconnection regions in the tail.

Brecht et al. (1981) studied the effects of an east-west component of the IMF being added to a solar wind carrying a -2γ southward field. This calculation was fully three-dimensional with no planes of symmetry

used. This was necessary to allow for the rotation of the IMF. The code used in-flow boundary conditions on the + x boundary and out-flow conditions on all other boundaries. The numerical scheme employed was a partial donor cell method (PDM), Hain (1978). PDM couples a low order numerical scheme to a high order scheme in a nonlinear fashion in order to prevent numerical oscillations while maintaining good accuracy and minimum numerical diffusion. The results showed that a rotation of the IMF toward an east-west direction rotated or skewed the entire magnetotail and produced an induced B_y in the plasma sheet of the size seen in the solar wind. These results were found to be consistent with experimental data; Hardy et al. (1979), Lui (1979), and in agreement with an analytic calculation by Cowley (1981).

The simulation by Wu et al. (1981) addressed the case where no IMF exists in the solar wind. They used a Rusanov numerical scheme to solve the MHD equations. The calculation was performed on a quadrant of the magnetosphere meaning that both the meridional and equatorial planes were planes of symmetry. Because of the symmetry planes no reconnection can occur due to numerical resistivity. The boundary conditions required out- flow at 45° from the x axis. The calculation reproduced, apart from the diffusion effects noted by the authors, many of the major features of the magnetosphere.

In this paper we present results of refined simulations where we consider the structure and dynamics of the magnetosphere in the presence of a - 2γ IMF. The paper will discuss in detail the calculational set up and equations used in the simulation. In addition, we present time resolved results of island formation in the tail and attendant flows and densities. Finally the conclusions derived from these simulations will be presented.

Calculation

As mentioned earlier in this paper, the code uses a PDM scheme for solving the MHD equations. This scheme allows resolution of shocks in 3 cells and therefore permits the use of fewer grid cells than is necessary for schemes where more numerical diffusion is present, for example, Lax or Rusanov. The MHD equations the code solves are

$$\frac{\partial \rho}{\partial t} = - \nabla \cdot \rho v$$

$$\frac{\partial \bar{v}}{\partial t} = - \bar{v} \cdot \nabla \bar{v} - \frac{1}{\rho} [\nabla (P + Q) + J/c \times B]$$

$$\frac{\partial P}{\partial t} = - \nabla \cdot P\bar{v} - (\gamma - 1)(P + Q) \nabla \cdot \bar{v} - \eta J^2$$

$$\frac{\partial \bar{B}}{\partial t} = - c \nabla \times \bar{E}$$

where $\bar{E} = - (v \times B)/c - \eta J$ and $\bar{J} = c \nabla \times \bar{B}/4\pi - \frac{\partial \bar{E}}{\partial t}$.

The variables ρ, v, P, B, η, and Q are mass density, velocity, plasma pressure, magnetic field, resistivity and artificial viscosity. Artificial viscosity is necessary to insure that the Rankine-Hugoniot relations are satified throughout the code. It is only activated in the region of the simulation where there is compressive flow, $\nabla \cdot \bar{v} < 0$. The PDM algorithm in conjunction with this set of equations guarantees that numerically $\bar{\nabla} \cdot \bar{B} = 0$ everywhere in the code, a critical feature to the validity of the simulation not automatically obtained by all schemes. The effect of high Alfven speeds in requiring unreasonably short time steps is controlled by the $\partial \bar{E}/\partial t$ term in Amperes' law. The inclusion of the displacement current effectively limits the propagation speed of the

Alfven waves to the speed of light, which can be arbitrarily set in the code. The boundary conditions for this simulation are the same as those used in our previous 3-D paper [Brecht et al., 1981]. The + X boundary has an inflow condition and all other boundaries have an outflow condition.

The simulation presented in this paper was performed on a grid using a stretched mesh of 29 x 21 x 21 cells in the x,y and z directions of the solar-magnetospheric coordinate system. The spatial extent of the numerical grid is $-100\ R_e \leq X \leq 30\ R_e$, $-40\ R_e < Y < 40\ R_e$ and $-40\ R_e < Z < 40\ R_e$. The earth's dipole field is formed by placing a current loop at X = Y = Z = 0 with the appropriate current to replicate the earth's field. A solar wind is then introduced into the calculation from the + x boundary, which distorts the dipole field and creates the magnetosphere. The solar wind may carry an IMF of any strength and orientation. The solar wind introduced into the calculation presented here has a velocity of 400 km sec^{-1}, a density of 5 cm^{-3} and a $B_z = -2\gamma$. The grid was initially loaded with a plasma density of 1 cm^{-3}.

Results

The results presented here are a 3-D time evolution calculation of the magnetosphere as a southward (-2γ) IMF interacts with the earth's magnetic field. Reconnection was permitted to occur in this simulation. We had the option of no reconnection, using real resistivity in the equation, or permitting numerical reconnection. We chose the latter case for several reasons. Foremost among these is the fact we did not know where to put the resistivity and in what amount. Arbitrary prescriptions did not appeal to us. Numerical resistivity occurs mainly where opposed fields are being driven together in a compressive fashion causing the location of reconnection regions to be determined by the dynamics of the calculation not the predisposition of the author. At this juncture of our research we are actively testing various ways to model the microinstabilities, Lyon et al. (1981b), which are thought to provide the necessary resistivity for the reconnection process. However the present, the proper physics and its implementation is not well resolved. It should be noted that for steady state configurations such as those used in the research of Birn and Hones (1981) the PDM scheme will not numerically reconnect. The numerical reconnection shown here is purely a driven phenomenon. One disadvantage of using numerical reconnection is that with this code there is no resistive heating of the plasma. Therefore, only the magnetic field and pressure forces caused by the compressive flow will affect the plasma dynamics. As will be shown in this paper these terms alone provide rather impressive effects in the earth's magnetotail.

The calculation begins with the earth's dipole field being acted upon by a solar wind of the previously stated properties as well as

the - 2γ southward IMF. A reconnection point forms in the near earth tail region approximately 4500 secs into the calculation. (In this paper all times quoted are real time and not computer simulation time). This reconnection point begins to move tailward. Eventually another reconnection point occurs and a magnetic island forms and begins to move in tailward direction. As this island moves tailward another island is formed. The general dynamics of the system is quite similar to the 2-D simulations reported by Lyon et al. (1981a) and the 3-D simulation by Birn and Hones (1981). One main difference in the results of the 2-D and 3-D simulations is that for the 3-D simulations strong earthward flows are observed whereas in 2-D this was not the case. It was speculated by Lyon et al. (1981a) that the lack of earthward flow could be due to the two-dimensionality of the calculation and this appears to be the case.

In figures 1 -5 the global temporal dynamics of the various plasma parameters are shown. Each set of figures begins at 7691 sec (0 min) into the calculation and run through 11351 secs (~ 65 min) and therefore cover slightly over one hour of real time. The beginning time was selected because most of the initial transients produced as the dipole field was transformed into a magnetospheric topology were out of the system. One remnant of such a transient is seen as a reversed field structure in the tail of the magnetosphere in Fig. 1 at about 55 R_e. In addition we have chosen two locations in the magnetotail at Y = 0, Z = 0, and X ~ - 19 R_e and - 32 R_e to display plasma properties that a satellite would detect during this time frame (Figs. 6 - 10).

Fig. 1 is a time sequence of magnetic vector plots on the x-z meridional plane. The vectors are normalized to the local magnitude of B, so the size of the vector provides no indication as to the strength of

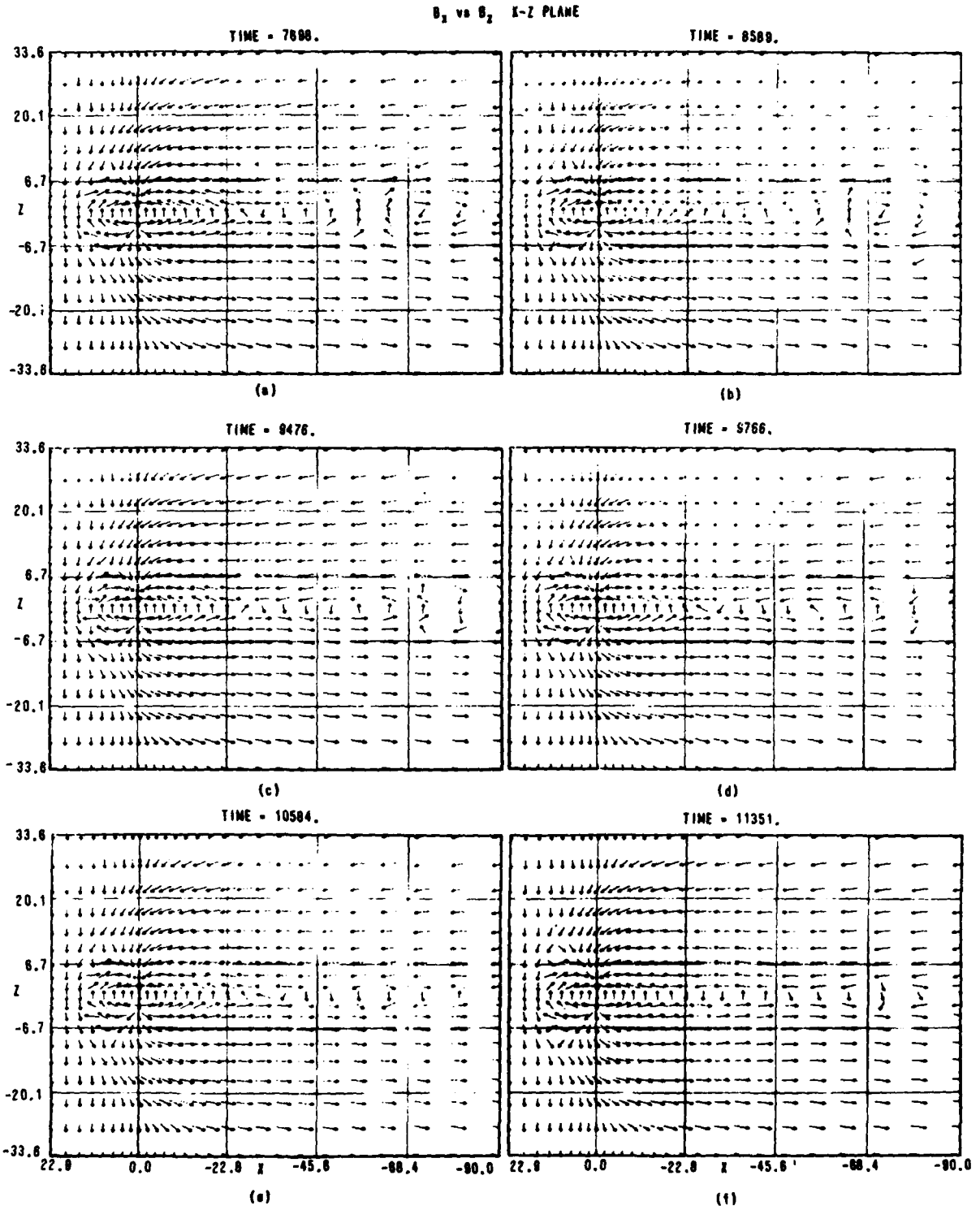

Fig. 1 — Time evolution of the B_x and B_z magnetic field components plotted in the meridional (noon-midnight) plane. For purposes of discussion 7698 and 11351 sec correspond to 0 min. and ~ 65 min. respectively. The length of the vector drawn provides no information about the magnitude of the fields. All distances are measured in earth radii.

the magnetic field. In Fig. 1a one notes the existence of a reconnection point at about -68 R_e in the tail as well as an o-point in the -35 R_e to - 40 R_e region. In the following several snapshots one sees the interior island grow in the tailward direction and by 9766 secs is beginning to accelerate tailward. The last timestep shows the formation of a new island with the inner x-point located at approximately -20 R_e in tail.

The velocities that correspond to the creation and motion of these sets of neutral lines or o-points can be seen in Fig. 2. Here we show the velocities in the equatorial, x-y plane. In these plots the arrow length indicates the magnitude of velocity. The unit vector is set to be 400 km sec^{-1}, the solar wind velocity. The general features of the magnetosphere can be see in Fig. 2a. The stagnation point in the bow is located at about X = 12 R_e, and the magnetopause can be seen draped around to the sides. In the interior region of the magnetotail one notes a demarcation line of very low velocities at X ~ - 29 R_e corresponding to the location of the x-point seen in the magnetic field plots at the same time. Earthward of this point there is flow toward the earth. Tailward of this point the flow is predominately away from the earth. It should be noted that in the meridional plane one sees these flow patterns restricted primarily to - 2 R_e < Z < 2 R_e. To a large extent the magnitude of the flow is determined by the mass loading of the magnetic field. The correspondence between high flow regions and low densities is quite high as can be seen in Fig. 2 and 4, which show the perspective plots of velocity and density in the equatorial plane.

As one scans through the various time steps shown in Fig. 2, one notes the velocities pulsate within a period of about 20-30 minutes. This is noticeable if one considers the X ~ - 22 R_e grid line shown in

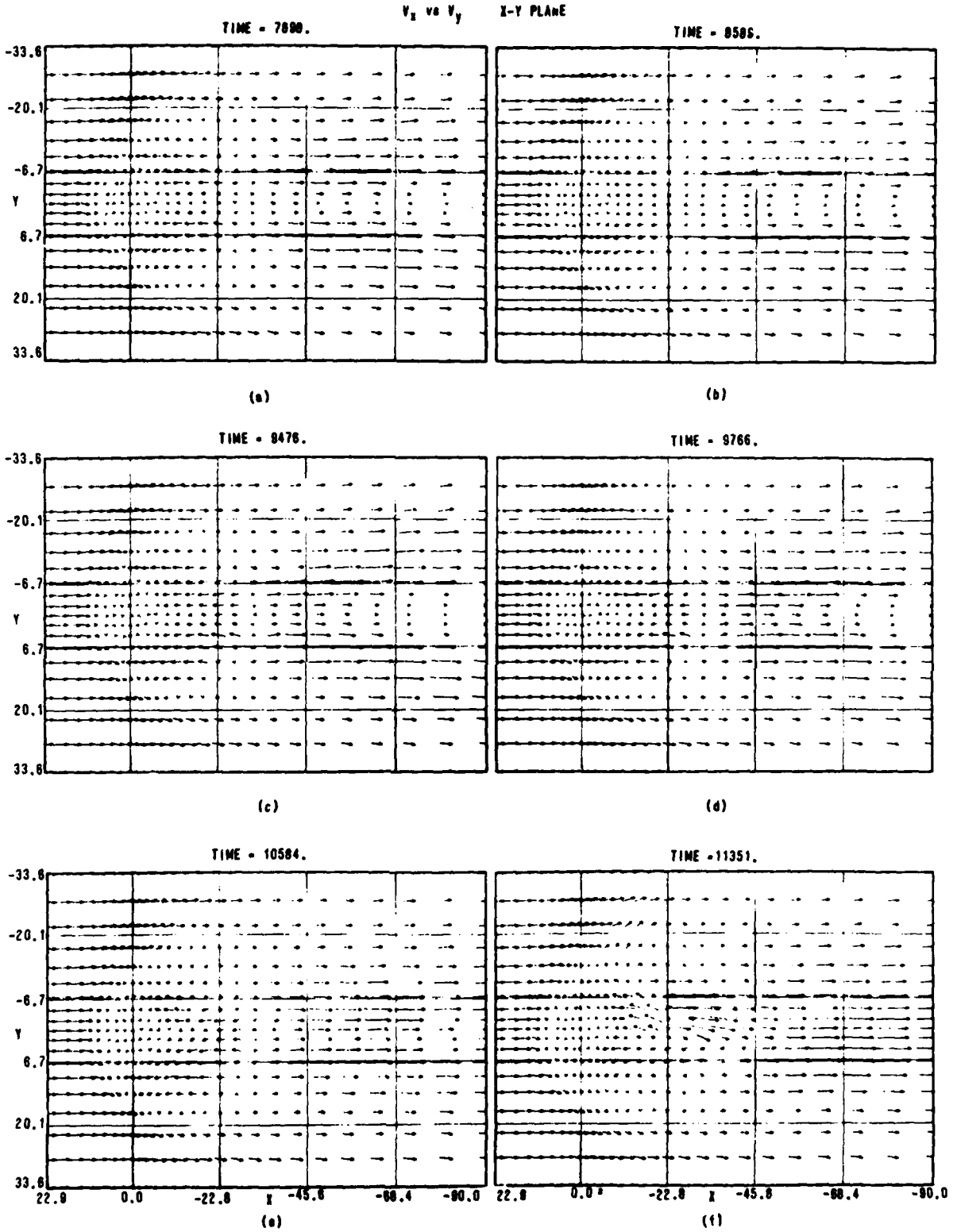

Fig. 2 — Time evolution of V_x and V_y velocities in the equatorial plane. The unit vector is 400 km sec^{-1} which is the solar wind velocity.

Fig. 2. As time progresses one notes two obvious features. The first is that the speed of the flows increases with time as successive islands are formed. This feature was noted in the 2-D simulation by Lyon et al. (1981a). In both calculations each succeeding reconnection event reduces the amount of mass on the field lines and consequently the flow speed becomes larger. Fig. 2f also shows the second feature, an asymmetry in the flow pattern. This is a particularly interesting feature caused by the motion of the x-point at the bow of the magnetosphere. Because of the large number of timesteps in this calculation numerical noise permitted the reconnection point on the bow to shift slightly. Once this occurs the continued flow begins to develop an asymmetry on the bow which manifests itself as motion in the tail and produced the asymmetic flow, much as one might expect in the real magnetosphere. The density and pressure are noted to be asymmetric. In this simulation the asymmetry existed in only the dawn - dusk direction. The fact that the reconnection point has become slightly asymmetric may be more realistic than the usual perfectly symmetric simulation. It should also be noted that the region of very rapid flow is restricted mainly to the equatorial plane, but as can be seen does, in fact, cover a large spatial region in both the x and y directions. The flow speeds reach velocities as high as 650 km sec^{-1} in the earthward direction and 800 km sec^{-1} tailward.

Coincident with the cycling of the island formation one can see considerable effects on the density and pressure in the magnetotail. Looking at the density in the meridional plane (Fig. 3) one sees two important features. The first is that, as the successive neutral lines move tailward the plasma sheet thins tremendously, and second that the plasma sheet density is considerably reduced. In Fig. 4f the density in

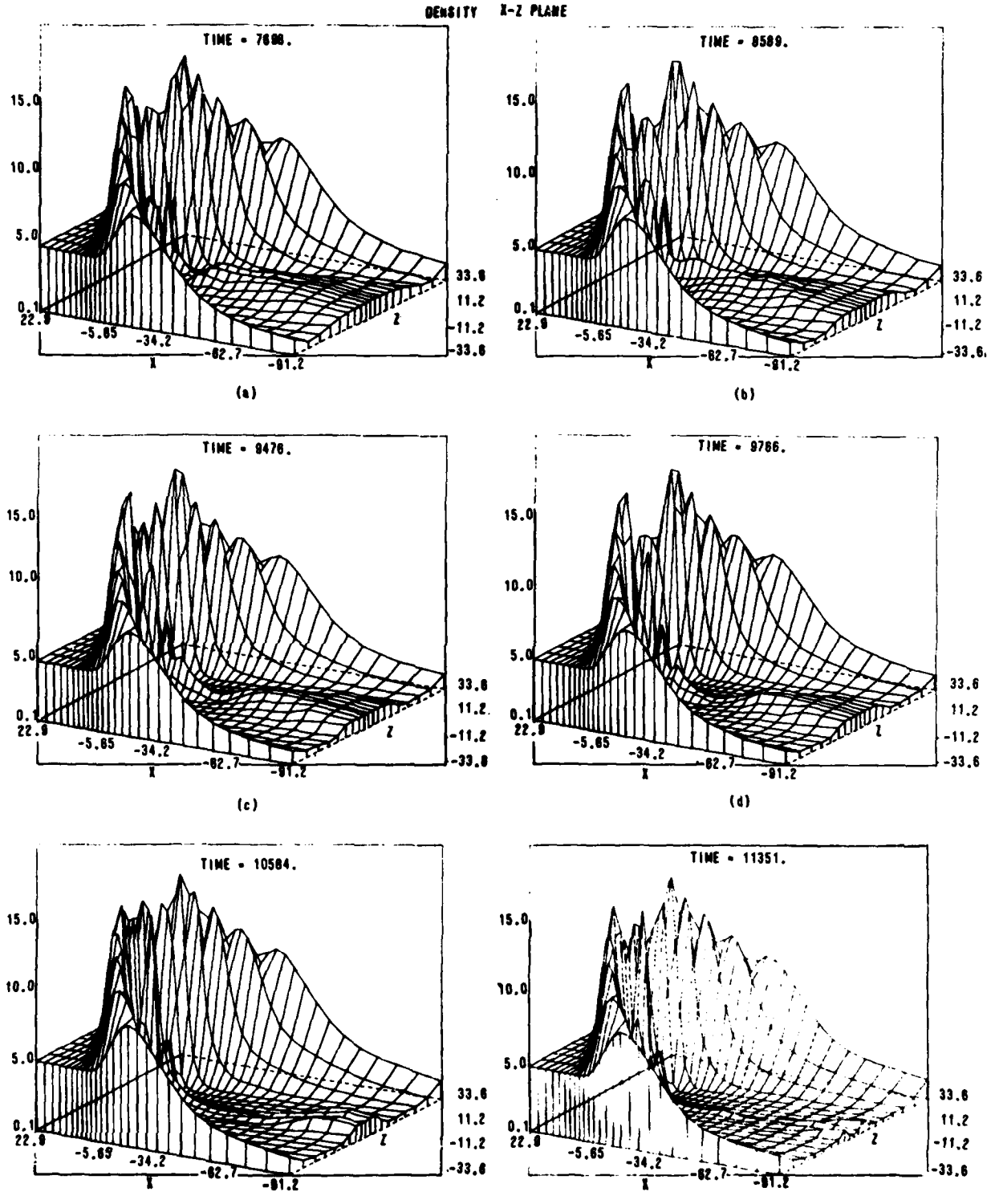

Fig. 3 — Perspective plots of density in the meridional plane. Units for the density scale are in particle cm^{-3}. The rather jagged appearance of the bow shock is due to the perspective plotter, not data. This is true for all perspective plots shown.

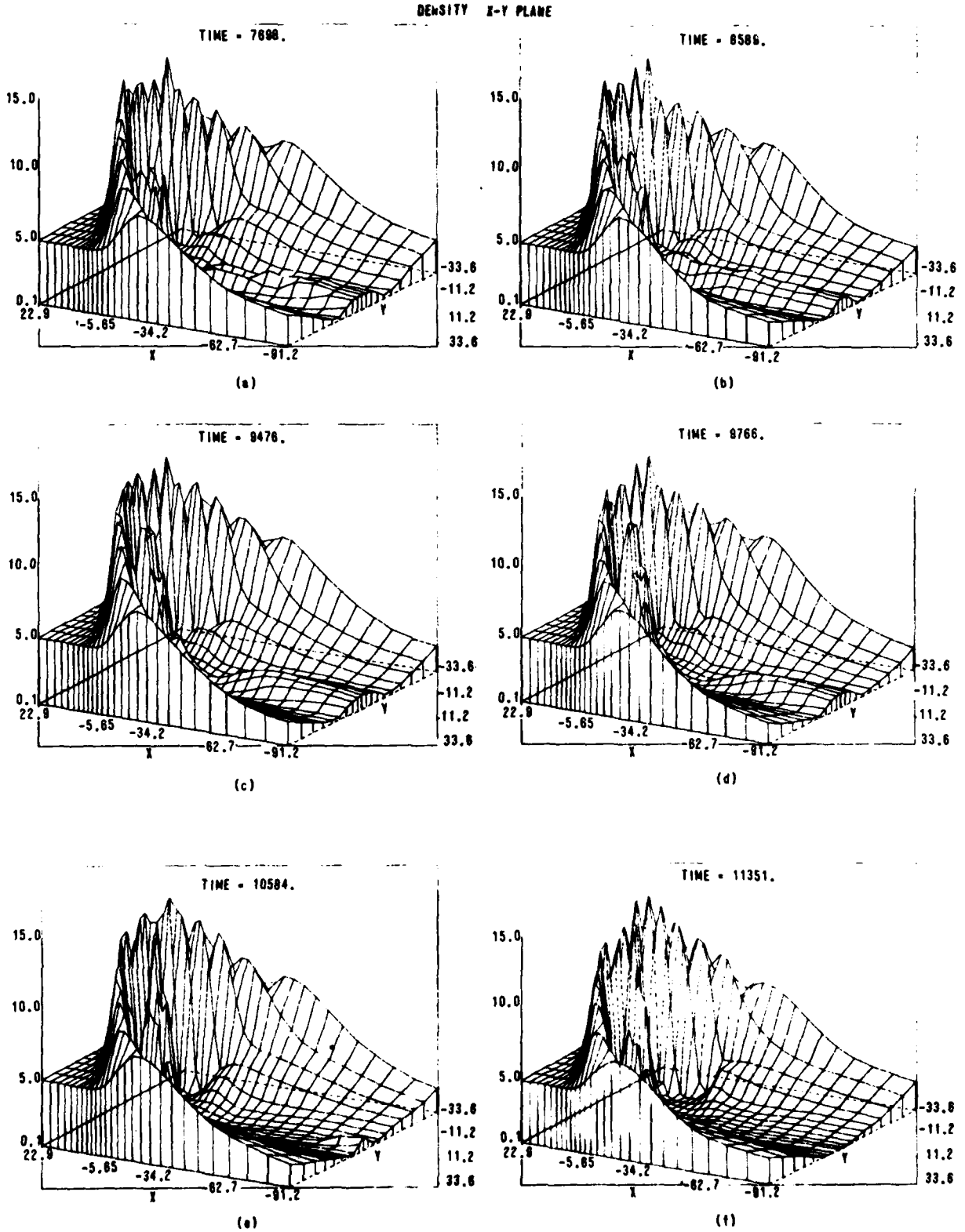

Fig. 4 — Perspective plots of density in the equatorial plane

the middle of the tail is quite low, but an enhancement of the density is occurring on the flanks of the tail. The asymmmetry caused by the shifted reconnection point is only about 10% in density from the dawn side to the dusk side. Fig. 5 shows the pressure in the meridional plane where one sees the rather dramatic sheet thinning often associated with reconnection events, Hones and Schindler (1979), and Hones (1979). In Fig. 5a-f one notes the progressive thinning of the sheet as indicated by the pressure dropout and a general overall reduction in pressure along the plasma sheet, Z = 0. Also, one notes a slight recovery of the pressure occurring inside of about X = - 20 R_e and moving tailward.

In the next several paragraphs we discuss data taken from the code at two locations in the magnetotail. The time resolution of the data is approximately 5 min intervals. In a sense this is plasma and field data as a satellite would detect it during the hour we have displayed. The two locations are located at Y = 0, Z = 0, X ~ - 19 R_e and - 32. R_e.

In Fig. 6 we show the x velocity as seen at the two locations mentioned above. The inner location sees an earthward flow which becomes progressively stronger with time. There is a slight oscillation in the velocity, but generally it is increasing. The maximum velocity is reached at about 55 min. At this time the magnetotail neutral line has moved to beyond the X ~ -32 R_e location, Fig. 1e. Shortly after this time the tail reconnects and a x-point forms at about X ~ -22 R_e, as can be seen on the B_z field evolution in Fig. 1f. The creation of the inward neutral line corresponds to the rather precipitous drop in velocity seen at the inner point. The outer location experiences an oscillating velocity of about 100 km sec^{-1}. During the outward stretching phase at about 55 min the tailward flow drops to about 50 km sec^{-1}. Locations

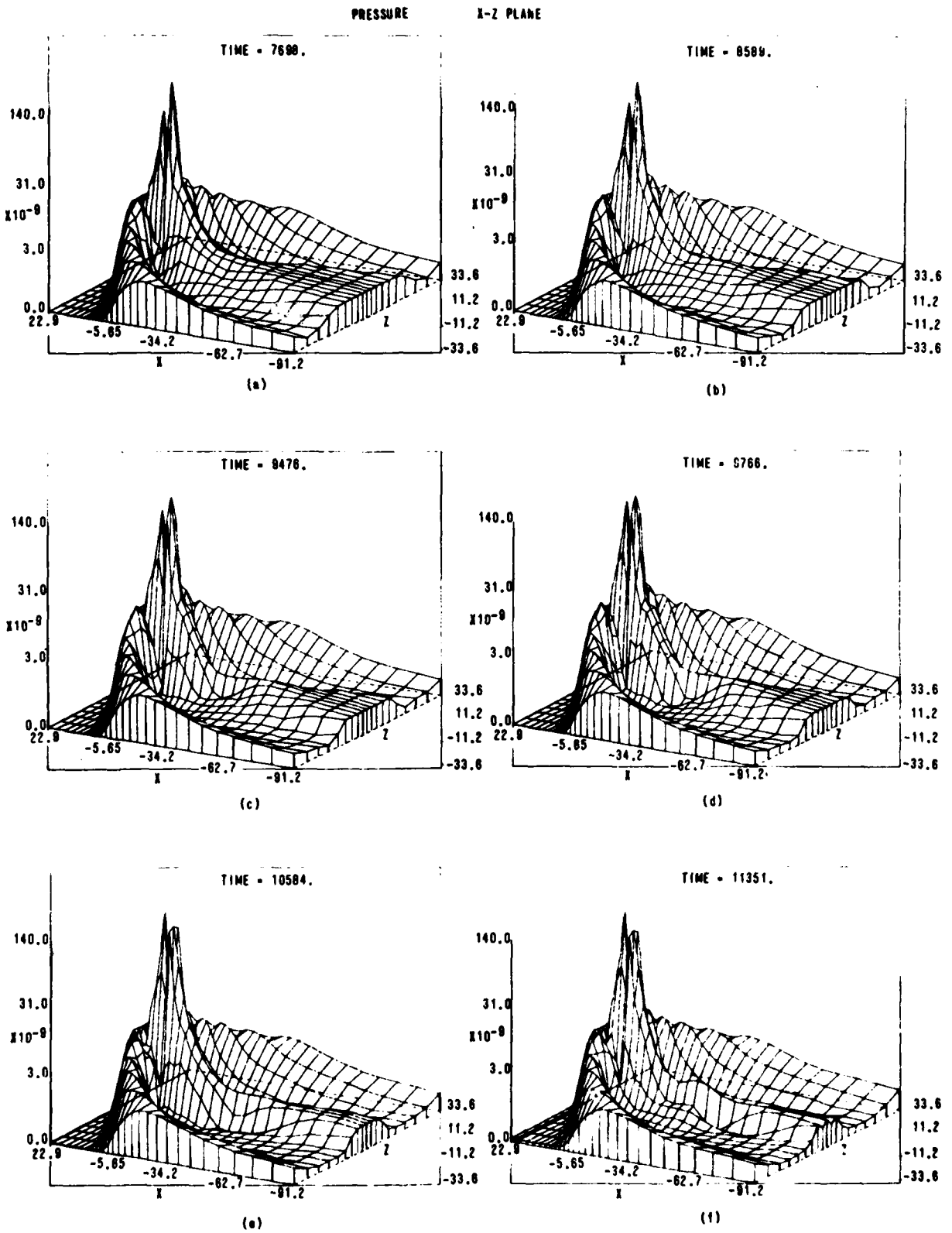

Fig. 5 — Perspective plots of pressure in the meridional plane. Units for the pressure scale are ergs cm^{-3}.

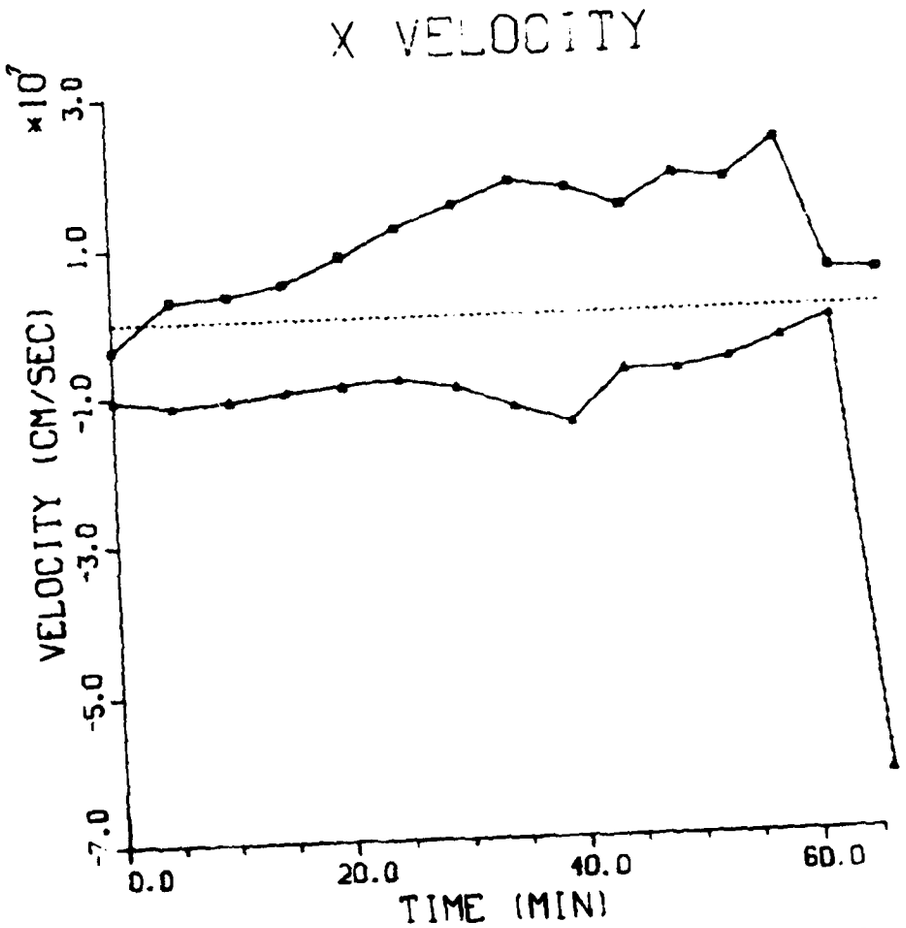

Fig. 6 — Temporal variations of V_x as seen at the locations X = - 19 R_e, Y = 0, Z = 0 denoted by squares and X = - 32 R_e, Y = 0, Z = 0 denoted by triangles

slightly closer to the earth experience a complete flow cycle from negative to positive and back to negative flow. As soon as the x-point forms earthward of the observation point one sees the tailward velocity go from -50 km sec^{-1} to -650 km sec^{-1} in less than 5 min. Similar to the results of Lui (1979) and Hones and Schindler (1979), strong dawn-dusk velocities are detected at these two locations. The inner point displayed primarily a duskward flow until the neutral line appeared at -22 R_e. At this time the flow changed rapidly to -300 km sec^{-1} in the dawnward direction. The outer point in the meantime displayed a constantly increasing duskward flow which peaked at -160 km sec^{-1}. The location of the observation point with respect to the neutral line seems to determine which direction the dawn-dusk flows go, Fig. 7. The z velocity generally stayed under 10 km sec^{-1} for both locations and oscillated between the positive and negative direction.

The B_x field was quite variable with the inner point experiencing larger fields as expected. The B_y field in these simulations remained negligible thoughout the simulation as detected at these locations. In Fig. 8, the time evolution plots of the z magnetic fields are displayed. Here one sees some very interesting behavior. The inner point experiences fairly large positive B_z components ranging from 5 to 8 gamma. However, at the time the neutral line is estabilished at ~ -22 R_e one sees a precipitous drop in the B_z component. This is caused by the close proximity of the neutral line. The outer point experiences more dynamic changes in B_z. Initially the neutral line is earthward of this point. One can correlate the expansion of the magnetic island seen in Fig. 1a-c with the general decrease of B_z from $\sim -1\gamma$ to $\sim -1.25\gamma$. The island then moves tailward and passes beyond the outer point as shown

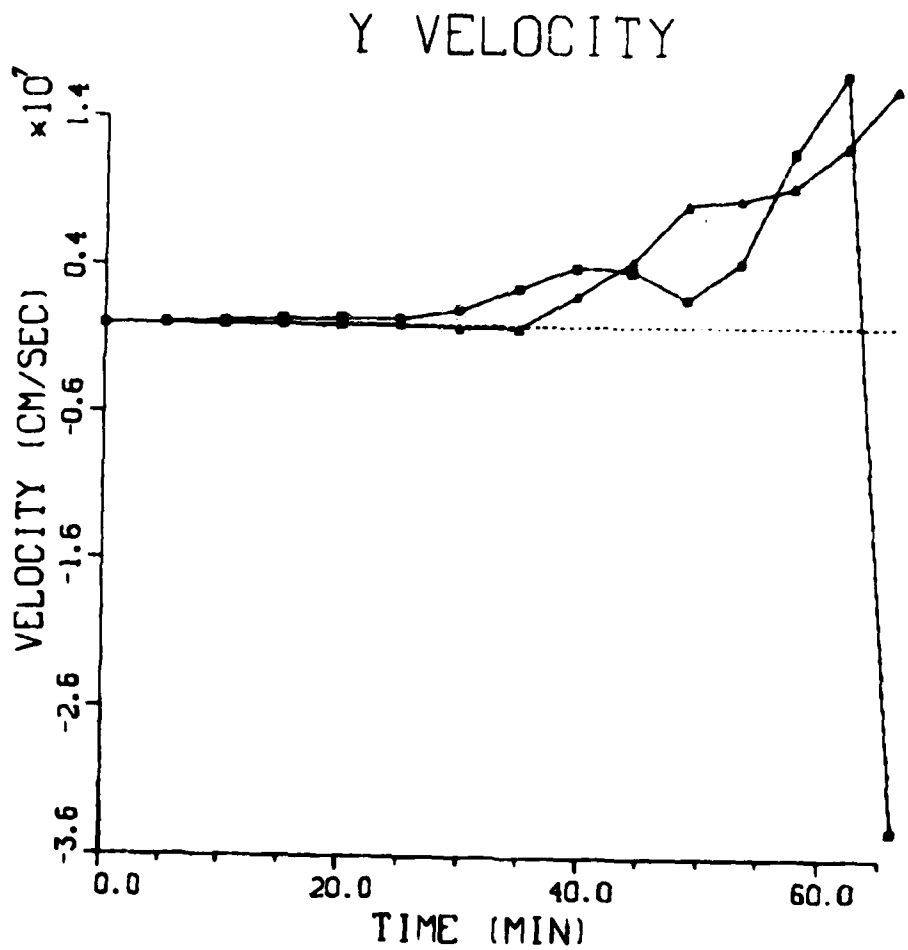

Fig. 7 — Temporal variations of V_y as seen by the two tailward locations. Squares indicate X = - 19 R_e and triangles X = - 32 R_e.

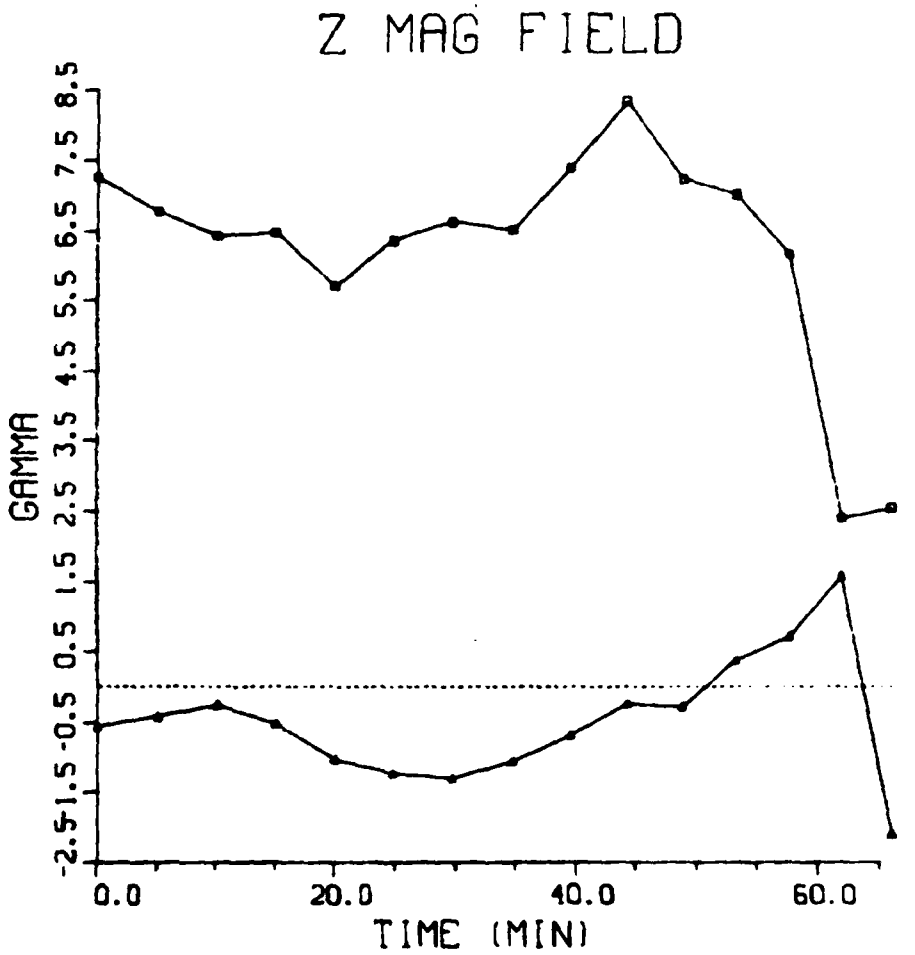

Fig. 8 — Temporal variations of B_z as seen by the two tailward locations. Squares indicate X = - 19 R_e and triangles X = - 32 R_e.

by the change of B_z from $\sim -1.25\gamma$ to $\sim 1.5\gamma$. As discussed earlier and coincident with the rapid increase of plasma flow a neutral line is established earthward of this point and the B_z changes from $\sim 1.5\gamma$ to $\sim -2\gamma$ in about the same 5 minute interval.

The relationship between the pressure, density and B_z component of the magnetic field is somewhat confused. Figure 9 shows that the two locations in the tail experience approximately the same pressure variation with perhaps a slight time delay. However, the formation of the new x-point causes the pressure behavior to change at about 65 min. At this time both locations show quite similar pressure levels. The inner location shows a drop of a factor of approximately two and the outer point is enhanced by about the same factor. In the density plot, Fig. 10, a build up of density occurs at about 20 min. Subsequent to this a general decline in density occurs. The build up is associated with the recovery of the plasma sheet from the passage of the previous island now located far in the tail, Figs. 1c and d. The decline in density after the 20 min mark is associated with the movement tailward of the o-point located at $X \sim -35\ R_e$, see Fig. 1d and e, and the associated stretching out of the tail. However, as can be seen the density plots do not display the variations seen in the pressure plots.

Comparing the pressure plots, Fig. 9, with magnetic field plots, Fig. 8, one notes that the outer location shows increases in pressure associated with decreases in the magnitude of B_z. This relationship holds until about the 60 min mark. By this time an x-point has passed by this location and a new one is about to form at $X \sim -22\ R_e$. The pressure is found to increase by a factor of about two. The magnitude of the B_z field passes through zero and ends up larger than it has been

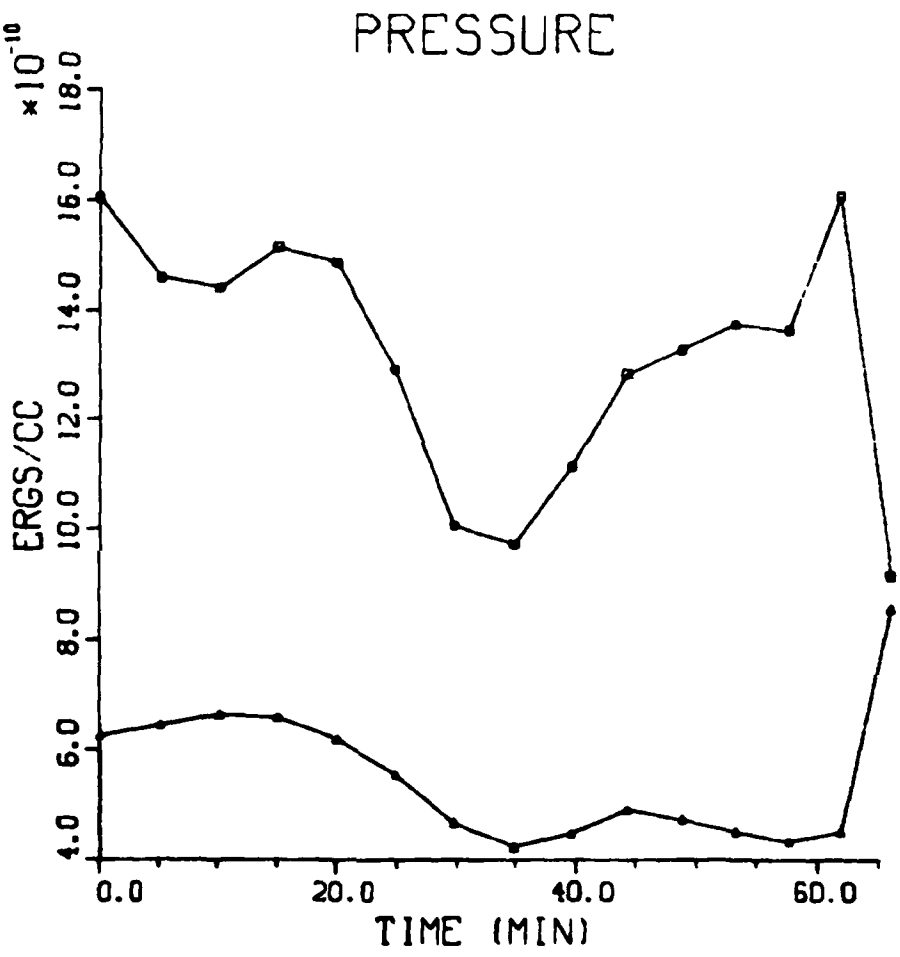

Fig. 9 — Pressure as a function of time for the location X = - 19 R_e (squares) and X = - 32 R_e (triangles)

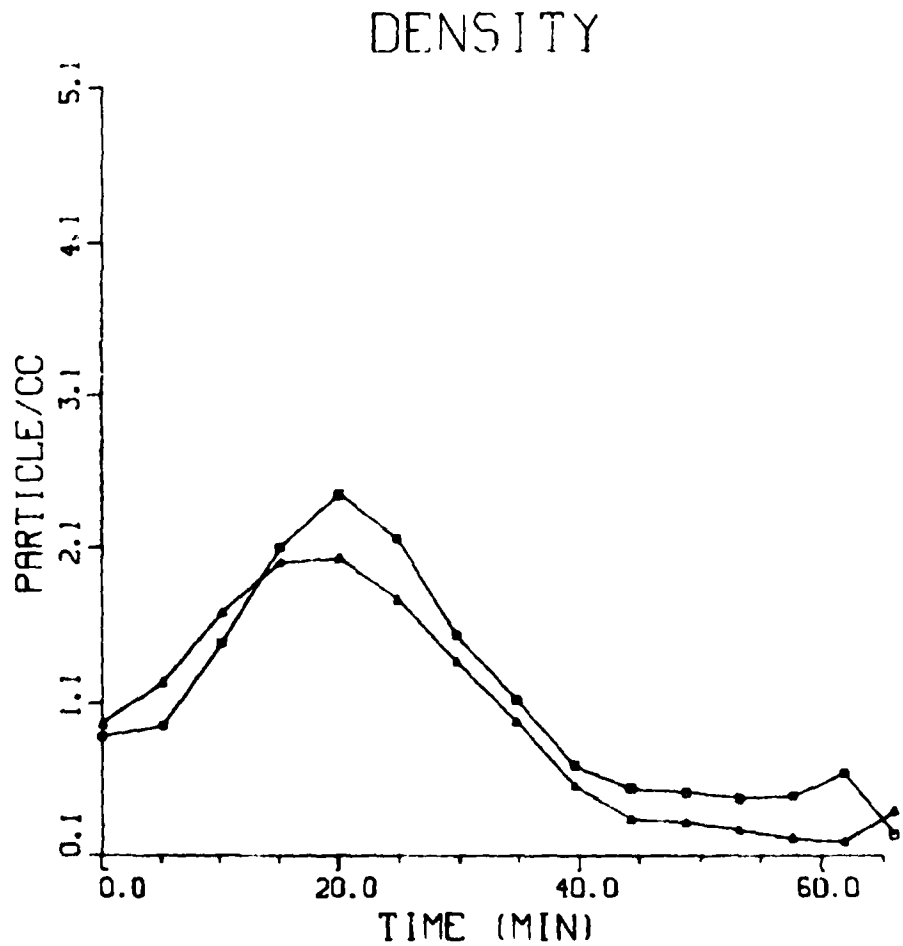

Fig. 10 — Density as a function of time for the locations $X = -19\ R_e$ (squares) and $X = -32\ R_e$ (triangles)

during this whole data sequence. The inner point exhibits different behavior. For the first 20 min the pressure and the magnitude of B_z follow one another. Then the pressure drops while B_z increases. During the final 30 min of data the two quantities then follow one another again. The correspondence of the density to either pressure or B_z is weak. Only the build up of density at 20 min appears to effect the variations seen in either the pressure or B_z.

These, then, are the basic results from the calculation. In the next section we discuss implications of these results and how they correlate with experimentally obtained data.

Discussion

While one encounters considerable difficulty in correlating in an exact fashion the published experimental results with those of a numerical simulation, the experimental results do provide a guideline to the kind of questions one ought to ask concerning the numerical results. There have been many articles published reporting satellite data from all areas of the magnetosphere during substorm events. However, for the purposes of this discussion we have restricted ourselves to the data reported from the IMP-6 satellite by Hones and Schindler (1979), and Lui (1979). It is not our intention, nor within our capability, to resolve differences between their respective analyses of the IMP-6 data. Our intention here is to compare the reported data with the calculation we have performed.

As discussed earlier we have selected and shown temporal data from various locations in the magnetosphere. The detailed data shown by Hones and Schindler (1979) are taken primarily in the $X \sim -30\ R_e$ region, but varies somewhat in the y and z direction. Lui (1979) displays detailed data in the same region, but shows not only data at $X \sim -30\ R_e$, but $X \sim -20\ R_e$ as well. In their statistical analysis the respective authors included data from all positions in x, subject to the various criteria placed on the data to determine its applicability.

At the risk of over- simplification of these authors' results one can sum up the major results in the following way. As a general rule the measured flows appeared to be field aligned. There appeared coincident with these events a dawn-dusk flow favoring the duskward direction. Lui (1979), arguing in favor of the current interruption model which we cannot assess with this particular calculation, reported that

statistically speaking there was not a strong correlation between negative B_z and tailward flow. Hones and Schindler (1979) found that for "40 - 50 percent of the events, no substorm effect on the flow is seen: in another 40 - 50 percent there is tailward flow associated with the substorms; and in 10 - 15 percent there is earthward flow". In addition, to comparing AE index to plasma flows, both Lui and Hones and Schindler also correlated plasma flow and sheet thinning. The respective authors reached apparently opposite conclusions based on their IMP-6 data for the relation between plasma sheet thinning and flow direction during a substorm.

Our calculations do not resolve the differences of these authors. For one thing it is not clear that the solar wind conditions in our simulation accurately represent the solar wind conditions that were present during the events for which these authors show data. As we have found earlier, [Brecht, et al. (1981)], inclusion of effects such as B_y in the solar wind makes considerable modifications to the magnetotail, not to mention the possible effects on microinstabilities thought to provide resistivity for tearing. We can, however, from our simulation either add to the confusion or provide some clarification, depending on the reader's point of view.

It is heartening to note that the magnitude of the quantities displayed in Figs. 6-10 are similar to those found in the magnetotail. We see in Fig. 8 variations and magnitudes of B_z consistent with the data shown by Lui (1979), see Figs. 14 and 16, which correspond with our selected observation data points. The velocities seen in our calculation are also consistent with those seen during substorm events. The pressures also appear to be consistent with the data albeit somewhat

lower, possibly due to the lack of ohmic heating expected to occur because of resistivity. We do not, however, see dropouts of several orders of magnitude in the data at Y = 0, Z = 0. Factors of five seem to be the most we see directly in the magnetotail. However, consideration of Figs. 3-5 show that any displacement from the central part of the plasma sheet either in y or z can result in considerable drop in either pressure or density.

We have found in this simulation that the data one collects is extremely dependent on location. Consider Fig. 2 at a position of Z = 0, $Y \sim > 6\ R_e$ and X between $-23\ R_e$ and $-45\ R_e$. One notes that if the satellite had been located here during the hour that several x-points existed in the tail virtually no flow modification would have been detected. This type of event was reported by Hones and Schindler (1979) at $Y = 10.6\ R_e$. However, at $Y < -6\ R_e$ during this same time one would have seen flows approaching 400 km sec^{-1}. At the point $X = -22.8\ R_e$ the displacement in y also changes the characteristics of the flow because of curvature of the neutral line itself. An additional feature of this calculation is the dependence on Z seen in terms of earthward and tailward flows. All the flows shown here are on the equatorial plane, $-2\ R_e < Z < 2\ R_e$. If one moves above or below the Z = 0 plane one quite frequently finds flows of smaller magnitude. These flows occurred in x locations where strong flows existed at Z = 0.

Simultaneous data taken at the two locations in the sheet show the effects of the x-point motion. In Fig. 8 one sees that the point at $X \sim -19\ R_e$ experiences variations in B_z, which remains positive although it drops in magnitude as the x-point forms close to it. The outer point sees a reversal in B_z as the x-point passes this location and then

returns to negative as the new x-point forms at ~ 22 R_e. Looking at Fig. 6 one sees that the inner point detects earthward flow most of the time, but the outer point sees only tailward flow, although the sign of B_z reversed. As the new x-point forms the tailward flow jumps to over - 600 km sec^{-1}. Not shown in these figures is a point located at X ~ - 27 R_e. Here an observer would not only experience reversal of B_z, but also reversal of the flow pattern from tailward to 100 km sec^{-1} earthward back to > 700 km sec^{-1} tailward. The point to be made is that during the passage of the x-point the dynamics of the new x-point formation caused the data to be extraordinarily sensitive to location. The existence of dusk-dawn flows were also found at our two data points. The flow was duskward for most of the simulation, but when the new x-point formed the outer location experienced a tremendous change. The flow went from 140 km sec^{-1} to - 350 km sec^{-1}. The pressure shows the type of plasma sheet dropouts seen in the data. However, one interesting point should be noted. As the neutral line approached the inner point at 65 min., the plasma pressure dropped along with the plasma flow speed and the magnitude of B_z. At the outer point the opposite result occurred at this time.

Finally, as reported by Lui (1979), and Hones and Schindler (1979) we find that most of the energetic flows appear to be field aligned. These flows are found to originate at the neutral line. In fact, they cannot be generated eleswhere because $\eta = 0$ and only J x B and pressure forces are in effect. A comparison of Figs. 1 and 2 illustrates this point. While Fig. 1 does not display magnetic field lines, B_y is typically an order of magnitude smaller than the other components.

In short, within this one simulation we find conditions and plasma

behavior quite similar to the various statistical features reported by Hones and Schindler (1979), and Lui (1979). Whether or not they would be detected depended entirely on the observer's locations in the magnetotail at the time of the substorm like event.

Conclusions and Summary:

The 3-D time dependent simulations of the magnetosphere presented in this paper display many of the features commonly associated with substorms. It was found that motion of the x-point caused plasma dropout to occur in the magnetotail. The flows seen in this calculation appeared to be oriented in a field aligned direction. The speed of flow was inversely related to the plasma density on the field line. As the simulation progressed the density declined in the tail and the flow speeds increased. The magnitude of these flows and of other plasma and magnetic parameters appears consistent with satellite data during substorm periods. However, until the mass on the field lines is removed, the reconnection events do not produce behavior that corresponds to the usual picture of substorms. This fact is reasonable because the local Alfven speed is a good estimate for the maximum velocities produced by reconnection. For plasma parameters typically found in the tail, $B \sim 20\ \gamma$ and $n \sim 1\ cm^{-3}$ the Alfven speed is 400 km/sec. In the neutral sheet the Alfven speed drops to 40 km/sec. Therefore, in order to have large scale accelerations one needs plasma-dropout to achieve the 500 - 1000 km sec^{-1} speeds reported for substorms. Thus, if the neutral line model for substorms is correct, our results indicate that reconnection is a necessary, but not sufficient condition for substorm formation.

The simulation exhibited the tendency for multiple x-points or neutral lines in the tail. This result is consistent with Lyon et. al., (1981). The inner x-point for the time segment shown here tended to remain at $\lambda \sim -27\ R_e$ in the tail until the o-point grew sufficiently. It then began to move tailward, stretching the tail. At this point in

time a new x-point was seen to form at $X \sim -20\ R_e$. An interesting aspect of the simulation was the temporal behavior at various locations in the tail. Due to the multiple x-point formation and the asymmetric flow caused by the x-point shift on the bow, it was found that almost all of the various categories of events reported by Lui (1979), and Hones and Schindler (1979) could be observed in this one simulation. The location that remained earthward of x-points experienced no field reversal nor a flow reversal in v_x as the various x-points were formed and moved tailward. Points shifted in y from Y = 0 often displayed no modification to plasma flow during these events. Yet as the flow moved toward the dawn side due to the shift in the bow reconnection point one found that at $Y < -6.7\ R_e$ flows were detected to coincide with the formation of the x-point while at $Y > 6.7\ R_e$ no effects were detected. Observation points were found in the tail at Y = 0, Z = 0, $X = -27\ R_e$ and $-32\ R_e$ which showed field reversal from negative B_z to positive B_z and a return to negative as a neutral line passed these locations and a new one was formed closer to the earth. These points experienced different flow behavior with the reversal of B_z. The point located at $X = -27\ R_e$ experienced reversals in the v_x direction consistent with the neutral point being either earthward or tailward of that point. The point at $X = -32\ R_e$ did not experience reversal of v_x, but only saw a reduction of the tailward flow. This lack of the flow reversal can probably be attributed to the formation of the x-point at $X \sim -20\ R_e$ within five minutes of the previous neutral line passage.

Finally, the various statistical categories used by Hones and Schindler (1979) and Lui (1979) to categorize plasma and magnetic behavior during the many substorm events experienced by IMP-6 appear to

be found in this one simulation. This leads one to the not so profound conclusion that, because of the complicated magnetotail behavior, spatial and temporal variations allow one to sample a full range of dynamic behavior determined primarily by the location of the observer.

Acknowledgement

This work was supported by the Office of Naval Research and NASA.

References

Akasofu, S.-I., A.T.Y. Lui, C.I. Meng, and M. Haurwitz, "Need for a three-dimensional analysis of magnetic fields in the magnetotail during substorms, Geophys. Res. Lett., 5, 283, 1978.

Birn, J., and E.W. Hones, "Three-dimensional computer modeling of dynamic reconnection in the geomagnetic tail", J. Geophys. Res., 86, 6802, 1981.

Boris, J.P., and D.L. Book, "Flux-corrected transport I: SHASTA, a transport algorithm that works, J. Comp. Phys., 11, 38, 1973.

Brecht, S.H., J.G Lyon, J.A. Fedder, and P.J. Palmadesso, "Comments on plasma dynamics in the earth's magnetotail", Comments on Plasma Physics and Controlled Fusion, 6, 59, 1980.

Brecht, S.H., J. Lyon, J.A. Fedder, and K. Hain, "A simulation study of east-west IMF effects on the magnetosphere", Geophys. Res. Lett., 8, 397, 1981.

Coroniti, F.V., L.A. Frank, D.J. Williams, R.P. Lepping, F.L. Scarf, S.M. Krimigis, and G. Gloeckler, "Variability of plasma sheet dynamics", J. Geophys. Res., 85, 2957, 1980.

Cowley, S.W.H., "Magnetospheric asymmetries associated with the y-component of the IMF", Planet. Space Sci., 29, 79, 1981.

Dungey, J.W., "Interplanetary magnetic field and the auroral zone", Phys. Rev. Lett., 6, 47, 1961.

Fairfield, D.H., "On the average configuration of the geomagnetic tail, "J. Geophys. Res., 84, 1950, 1979.

Hain, K., "The partial donor cell method," NRL Memorandum Report, No. 3713, 1978.

Hardy, D.A., H.K. Hills, and J.W. Freeman, "Occurrence of the lobe plasma at lunar distances", J. Geophys. Res., 84, 72, 1979.

Hones, E.W., Jr. "Plasma flow in the plasma sheet and its relation to substorms", Radio Sci., 8, 979, 1973.

Hones, E.W., Jr., and K. Schindler, "Magnetotail plasma flow during substorms: A survey with IMP6 and IMP8 satellites", J. Geophys. Res., 84, 7155, 1979.

Hones, E.W., Jr., "Transient phenomena in the magnetotail and their relation to substorms", Space Sci. Rev., 23, 395, 1979.

Lax, P.D., "Weak solution of nonlinear hyperbolic equations and their numerical computation", Communication on Pure and Applied Math., 17, 159, 1954.

LeBoeuf, J.N., T. Tajiima, C.F. Kennel, and J.M. Dawson, "Global simulations of the time-dependent magnetosphere, Geophys. Res. Lett., 5, 609, 1978.

LeBoeuf, J.N., T. Tajima, C.F. Kennel, and J.M. Dawson, "Global simulations of the three-dimensional magnetosphere", Geophys. Rev. Lett., 8, 257, 1981.

Lui, A.T.Y., C.-I. Meng, and S.-I. Akasofu, "Wave nature of the magnetotail neutral sheet", Geophys. Res. Lett., 5, 279, 1978.

Lui, A.T.Y., "Observations on plasma sheet dynamics during magnetospheric substorms", Dynamics of the Magnetosphere, 563-597, Reidel Pub. Co., 1979.

Lyon, J., S.H. Brecht, J.A. Fedder, and P.J. Palmadesso, "The effect on the earth's magnetotail from shocks in the solar wind", Geophys. Res. Lett., 7, 712, 1980.

Lyon, J., S.H. Brecht, J.D. Huba, J.A. Fedder, and P.J. Palmadesso, "Computer simulation of a geomagnetic substorm", Phys. Rev. Lett., 46, 1038, 1981(a).

Lyon, J.G., S.H. Brecht, and J.A. Fedder, "An MHD simulation study of the factors controlling substorms", EOS, Tran. Am. Geophys. EOS., 62, 355, 1981(b).

McPherron, R.L., C.T. Russell, and M.P. Aubry, "Phenomenological model for substorms", J. Geophys. Res., 78, 3131, 1973.

Wu, C.C., R.J. Walker, and J.M. Dawson, "A three-dimensional MHD model of the earth's magnetosphere", Geophys. Res. Lett., 8, 525, 1981.

Zalesak, S.T., "Fully multidimensional flux-conected transport algorithms for fluids", J. Comp. Phys., 31, 335, 1979.

DISTRIBUTION LIST

Director
Naval Research Laboratory
Washington, D.C. 20375
Attn: T. Coffey (26 copies)
J. Brown
S. Ossakow (100 copies)

University of Alaska
Geophysical Institute
Fairbanks, Alaska 99701
Attn: Library

University of Arizona
Dept. of Planetary Sciences
Tucson, Arizona 85721
Attn: J. R. Jokipii

University of California, S. D.
LaJolla, California 92037
(Physics Dept.):
Attn: J. A. Fejer
T. O'Neil
Vu Yuk Kuo
J. Winfrey
Library
J. Malmberg
(Dept. of Applied Sciences):
Attn: H. Booker

University of California
Los Angeles, California 90024
(Physics Dept.):
Attn: J. M. Dawson
B. Fried
J. G. Moralles
Y. Lee
A. Wong
F. Chen
Library
R. Taylor
(Institute of Geophysics and
Planetary Physics):
Attn: Library
C. Kennel
F. Coroniti

Columbia University
New York, New York 10027
Attn: R. Taussig
R. A. Gross

University of California
Berkeley, California 94720
(Space Sciences Laboratory):
Attn: Library
M. Hudson
(Physics Dept.):
Attn: Library
A. Kaufman
C. McKee
(Electrical Engineering Dept.):
Attn: C. K. Birdsall

University of California
Physics Department
Irvine, California 92664
Attn: Library
G. Benford
N. Rostoker
C. Robertson
N. Rynn

California Institute of Technology
Pasadena, California 91109
Attn: R. Gould
L. Davis, Jr.
P. Coleman

University of Chicago
Encrico Fermi Institute
Chicago, Illinois 60637
Attn: E. N. Parker
I. Lerche
Library

University of Colorado
Dept. of Astro-Geophysics
Boulder, Colorado 80302
Attn: M. Goldman
Library

Cornell University
Laboratory for Plasma Physics
Ithaca, New York 14850
Attn: Library
R. Sudan
B. Kusse
H. Fleischmann
C. Wharton
F. Morse
R. Lovelace

Harvard University
Cambridge, Massachusetts 02138
Attn: Harvard College Observatory (Library)
G. S. Vaina
M. Rosenberg

Harvard University
Center for Astrophysics
60 Garden Street
Cambridge, Massachusetts 02138
Attn: G. B. Field

University of Iowa
Iowa City, Iowa 52240
Attn: C. K. Goertz
G. Knorr
D. Nicholson

University of Houston
Houston, Texas 77004
Attn: Library

University of Michigan
Ann Arbor, Michigan 48104
Attn: E. Fontheim

University of Minnesota
School of Physics
Minneapolis, Minnesota 55455
Attn: Library
J. R. Winckler
P. Kellogg

M.I.T.
Cambridge, Massachusetts 02139
Attn: Library
(Physics Dept.):
Attn: B. Coppi
V. George
G. Bekefi
T. Dupree
R. Davidson
(Elect. Engineering Dept.):
Attn: R. Parker
A. Bers
L. Smullin
(R. L. E.):
Attn: Library
(Space Science):
Attn: Reading Room

Northwestern University
Evanston, Illinois 60201
Attn: J. Denevit

Princeton University
Princeton, New Jersey 08540
Attn: Physics Library
Plasma Physics Lab. Library
M. Rosenbluth
C. Oberman
F. Perkins
T. K. Chu
V. Aranasalan
H. Hendel
R. White
R. Kurlsrud
H. Furth
M. Gottlieb
S. Yoshikawa
P. Rutherford

Rice University
Houston, Texas 77001
Attn: Space Science Library
R. Wolf

University of Rochester
Rochester, New York 14627
Attn: A. Simon

Stanford University
Institute for Plasma Research
Stanford, California 94305
Attn: Library
F. W. Crawford

Stevens Institute of Technology
Hoboken, New Jersey 07030
Attn: R. Rosen
G. Schmidt
M. Seidl

University of Texas
Austin, Texas 78712
Attn: W. Drummond
V. Wong
D. Ross
W. Horton
D. Choi
R. Richardson
G. Leifeste

TRW Systems Group
Space Science Dept.
One Space Park
Redondo Beach, California 90278
Attn: R. Fredericks
F. Scarf

National Science Foundation
Atmospheric Research Section (ST)
Washington, D.C. 20550
Attn: D. Peacock

Benson, Robert
Code 620
Goddard Space Flight Center
Greenbelt, Maryland 20771

Cauffman, David
NASA Headquarters
Code ST-5
Washington, D.C. 20546

Chang, Tien
Boston College
20 Demar Road
Lexington, Maryland 02173

Gendrin, Roger
CNET
3 Ave. do la Republique
Issy-les-Moulineaux,
FRANCE 92131

Heyverts, J.
Observatoire
D.A.F. G21G0
Meudon,
FRANCE

Kikuchi, Hiroshi
College of Sci. & Tech.
Nihon University
8, Kanda Surugadai, 1-chome, Chiyoda-ku
Tokyo,
JAPAN 101

deKluiver, H.
FOM-Institute Plasma Physics
P. O. Box 7
3430 AA Nieuwegein,
HOLLAND

Klumpar, David
Center for Space Sciences
P. O. Box 688
University of Texas
Richardson, Texas 75080

Leung, Philip
Dept. of Physics
University of California
405 Hilgard Avenue
Los Angeles, California 90024

Linson, Lewis
Science Applications, Inc.
P. O. Box 2351
LaJolla, California 92037

Lysak, Robert
Space Sciences Lab.
University of California
Berkeley, California 94720

Rodriguez, Paul
Phoenix Corp.
1600 Anderson Road
McLean, Virginia 22102

Schulz, Michael
Aerospace Corp.
A6/2451, P. O. Box 92957
Los Angeles, California 90009

Shawhan, Stanley
Dept. of Physics & Astronomy
University of Iowa
Iowa City, Iowa 52242

Temerin, Michael
Space Science Lab.
University of California
Berkeley, California 94720

Vlahos, Loukas
Dept. of Physics
University of Maryland
College Park, Maryland 20742

Wright, Bradford
Los Alamos Scientific Laboratory
Mail Stop 650
Los Alamos, New Mexico 87545

Wu, Ching Sheng
Inst. of Physical Sci. and Tech.
University of Maryland
College Park, Maryland 20742

Matthews, David
IPST
University of Maryland
College Park, Maryland 20742

Zanetti, Lawrence
Applied Physics Lab.
SIP/Johns Hopkins Road
Laurel, Maryland 20810

National Technical Information Center
Cameron Station
Alexandria, VA 22314

(12 copies if open publication,
otherwise 2 copies)
12CY Attn TC


DAT
ILM